



Optimization of Triarylpyridinone Inhibitors of the Main Protease of SARS-CoV-2 to Low-Nanomolar Antiviral Potency

Chun-Hui Zhang,[▽] Krasimir A. Spasov,[▽] Raquel A. Reilly, Klarissa Hollander, Elizabeth A. Stone, Joseph A. Ippolito, Maria-Elena Liosi, Maya G. Deshmukh, Julian Tirado-Rives, Shuo Zhang, Zhuobin Liang, Scott J. Miller, Farren Isaacs, Brett D. Lindenbach, Karen S. Anderson,* and William L. Jorgensen*

Cite This: *ACS Med. Chem. Lett.* 2021, 12, 1325–1332

Read Online

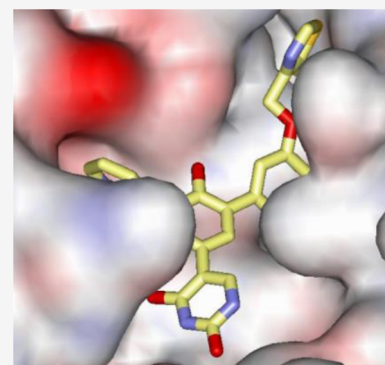
ACCESS |

Metrics & More

Article Recommendations

Supporting Information

ABSTRACT: Non-covalent inhibitors of the main protease (M^{pro}) of SARS-CoV-2 having a pyridinone core were previously reported with IC_{50} values as low as $0.018 \mu M$ for inhibition of enzymatic activity and EC_{50} values as low as $0.8 \mu M$ for inhibition of viral replication in Vero E6 cells. The series has now been further advanced by consideration of placement of substituted five-membered-ring heterocycles in the S4 pocket of M^{pro} and N-methylation of a uracil ring. Free energy perturbation calculations provided guidance on the choice of the heterocycles, and protein crystallography confirmed the desired S4 placement. Here we report inhibitors with EC_{50} values as low as $0.080 \mu M$, while remdesivir yields values of 0.5 – $2 \mu M$ in side-by-side testing with infectious SARS-CoV-2. A key factor in the improvement is enhanced cell permeability, as reflected in PAMPA measurements. Compounds **19** and **21** are particularly promising as potential therapies for COVID-19, featuring IC_{50} values of 0.044 – $0.061 \mu M$, EC_{50} values of ca. $0.1 \mu M$, good aqueous solubility, and no cytotoxicity.



KEYWORDS: SARS-CoV-2, protease inhibitors, lead optimization, COVID-19 drugs

Infection by SARS-CoV-2, the coronavirus responsible for the COVID-19 pandemic,¹ can be expected to be a serious world-health problem for many years.^{2,3} Though the rapid development and efficacy of vaccines have been impressive, a substantial fraction of the world's population will remain unvaccinated, and the continuing emergence of viral variants may add further challenges. Thus, it is important to develop alternative therapies for people who become infected with SARS-CoV-2.^{1–3} Among the potential viral targets, the chymotrypsin-like or main protease, M^{pro} , is particularly attractive.^{4,5} It is essential for viral reproduction because of its cleavage of polyproteins that are produced from ribosomal processing of the viral RNA, and its mutation rate is low, with 96% sequence homology between the 2002 SARS-CoV isoform and the 2019 SARS-CoV-2.⁶ In contrast to the common design of peptide-like covalent inhibitors for cysteine proteases, including SARS-CoV-2,^{4,5} we have pursued non-peptidic, non-covalent inhibitors.^{7,8} These alternatives are anticipated to display reduced potential for proteolytic degradation and induction of toxicities from off-target modification of proteins or nucleic acids.⁹

The research started from a virtual screen of ca. 2000 known, approved drugs that led to the identification of 14 drugs as inhibitors of SARS-CoV-2 M^{pro} with IC_{50} values as low as $5 \mu M$.⁷ One hit, the antiepileptic drug perampanel (**1**) (Figure 1), was chosen for lead optimization using computer-aided design, synthesis, a kinetic assay measuring enzyme inhibition, and

protein crystallography.⁸ The optimization rapidly delivered inhibitors with IC_{50} values as low as $0.018 \mu M$. Subsequent testing using infected Vero E6 cells showed that several of the inhibitors had similar antiviral potencies as the FDA-approved drug remdesivir, with EC_{50} values of ca. $1 \mu M$. Further optimization is described here, with emphasis on placement of a five-membered-ring heterocycle in the S4 pocket of M^{pro} and of regulation of cell permeability for the antiviral activity. New inhibitors are reported that have EC_{50} values as low as $0.08 \mu M$ and auspicious pharmacological properties.

In the prior work, we reported two subseries of analogues, one containing a cyanophenyl substituent, as in parampanel, and the other a uracilyl group.⁸ Compounds 2–4 and 5–7 in Figure 1 are examples. For these compounds, model building and crystallography demonstrated that the 3-pyridyl group resides in the S1 pocket of M^{pro} , the cyanophenyl or uracil ring in the S1' pocket, the chlorophenyl group in the S2 pocket, and the alkoxy substituent in the S3–S4 channel. Though parampanel is only a weak inhibitor, with an IC_{50} value of $>100 \mu M$, 2–7 yielded IC_{50}

Received: June 7, 2021

Accepted: July 13, 2021

Published: July 14, 2021



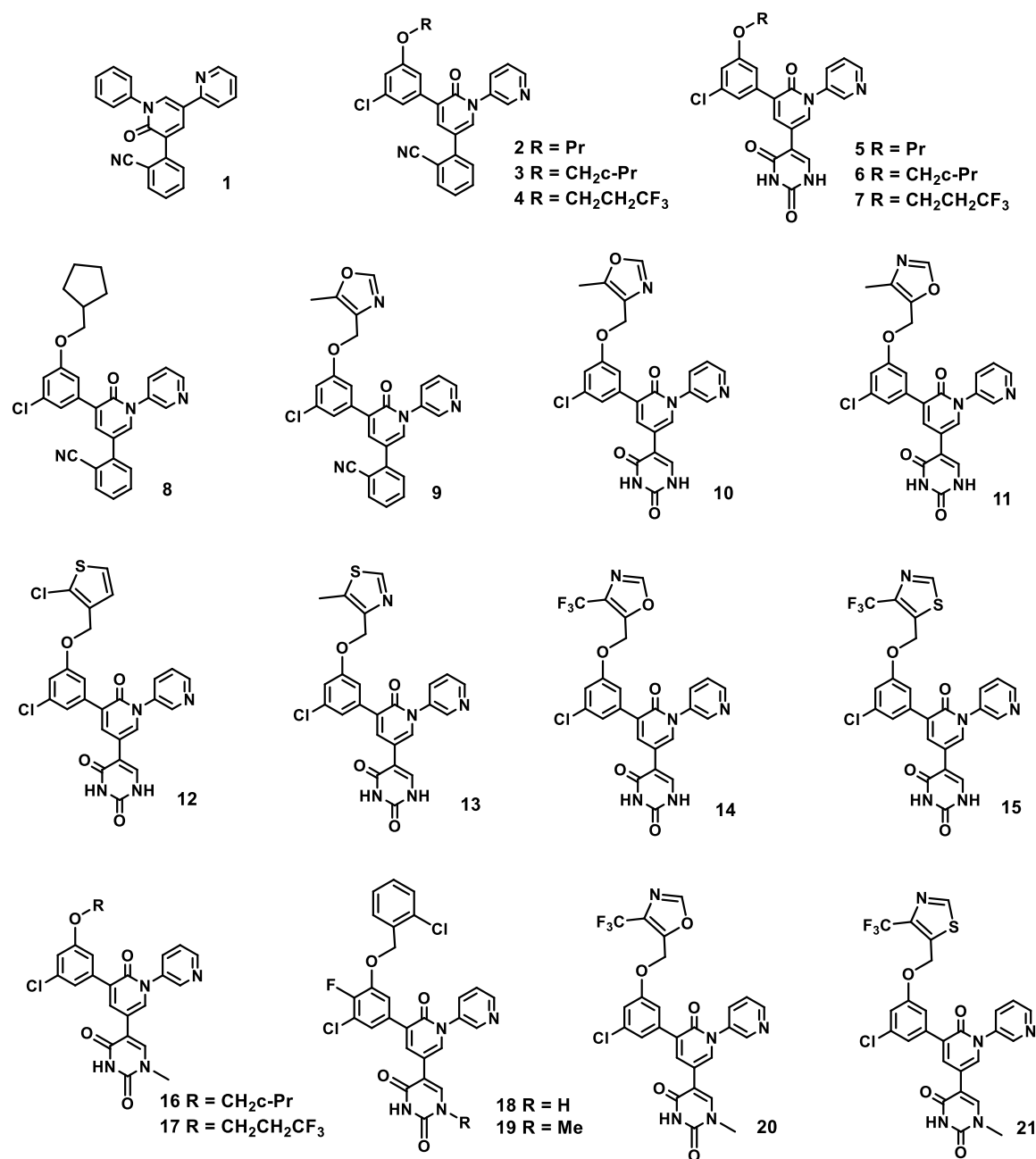


Figure 1. Inhibitors of SARS-CoV-2 M^{Pro}. 8–17 and 19–21 are new compounds.

Table 1. Measured Activities for Inhibition of SARS-CoV-2 M^{Pro}

compd	IC ₅₀ (μM)	compd	IC ₅₀ (μM)	compd	IC ₅₀ (μM)
1	100–250 ^a	8	0.328 ± 0.061	15	0.038 ± 0.015
2	0.140 ± 0.020	9	0.083 ± 0.023	16	0.061 ± 0.007
3	0.170 ± 0.022	10	0.085 ± 0.005	17	0.059 ± 0.014
4	0.120 ± 0.006	11	0.131 ± 0.009	18	0.028 ± 0.007
5	0.120 ± 0.016	12	0.027 ± 0.004	19	0.044 ± 0.009
6	0.037 ± 0.004	13	0.042 ± 0.015	20	0.130 ± 0.018
7	0.025 ± 0.003	14	0.105 ± 0.013	21	0.061 ± 0.011

^aFluorescence of the compound interfered with the assay.

values of 0.025–0.170 μM, as summarized in Table 1. The results were sensitive to the group that terminates in the S4 site: 3,3,3-trifluoropropoxy and *o*-chlorobenzoyloxy substituents yielded the most potent inhibitors, with IC₅₀ values near 0.020

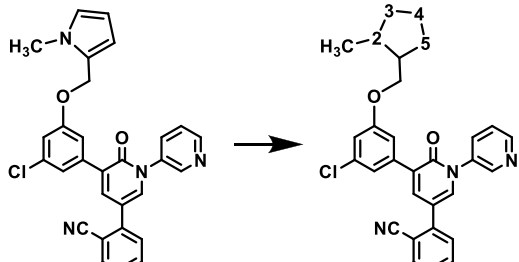
μM in the uracil subseries; the corresponding compounds in the cyanophenyl subseries are generally 2–3-fold less potent.⁸

Subsequent modeling considered replacement of the R group in the alkoxy substituent with five-membered-ring heterocycles.

Reduced torsional degrees of freedom and potential modulation of solubility and metabolic stability were viewed as possible benefits. The standard modeling consisted of structure building of the protein–ligand complexes with the BOMB program¹⁰ followed by conjugate-gradient optimization of the complexes using the MCPRO program¹¹ with the OPLS-AA/M force field for the protein,¹² the OPLS/CM1A force field for the ligand,^{13,14} and a dielectric constant of 2. The results indicated that a methyl group or a chlorine atom at the 2-position in the heterocycle should project well into the S4 site of M^{Pro}, as for the terminal carbon atom in the alkoxy groups of 2–7.⁸ Free energy perturbation (FEP) calculations were then used to assess more reliably relative binding affinities of alternative heterocycles.^{10,15–17} These calculations included the surrounding water molecules and extensive configurational sampling of the protein, ligand, and water. The FEP calculations were carried out starting with the BOMB-built structures and using standard protocols with the MCPRO program and the above-mentioned force fields.^{8,10} Relative free energies of binding, $\Delta\Delta G_b$, were obtained by mutating the ligand from structure A to structure B for both the protein–ligand complex in water and the unbound ligand. The configurational sampling for the systems was carried out at 25 °C with Monte Carlo simulations including the 242 protein residues nearest to the active site and 1250 and 2000 TIP4P water molecules¹⁸ for the ligand-bound and ligand-free calculations, respectively, as previously described.⁸

The FEP calculations were initiated from an *N*-methylpyrrol-2-ylmethoxy analogue, as summarized in Table 2. The

Table 2. Computed Changes in Free Energy of Binding (in kcal/mol) for Conversion of Five-Membered-Ring Heterocycles^a



2N to	$\Delta\Delta G_b$	2N to	$\Delta\Delta G_b$
2N	0.0	2N3N	1.33
3O	-0.24	2N4N	-0.05
4O	0.42	2N5N	-1.99
5O	-1.61	3N5O	-1.74
3S	-0.16	3N5S	-3.20
4S	0.76	5N3O	-1.15
5S	-2.11	5N3S	0.28

^aStatistical uncertainties from independent runs were ± 1 kcal/mol.

cyanophenyl series was modeled with the expectation that the relative results for the uracil series would be similar. The reference compound was converted to the six possible furan and thiophene analogues, a pyrazole, and the 2- and 5-imidazoles in an 11-window perturbation series. The 2- and 3-furan (5O and 3O) and thiophene (5S and 3S) analogues were then converted to the corresponding oxazoles and thiazoles. In all, 14 possible heterocycles were considered (Table 2). Since the uncertainties in the results from independent runs were ca. ± 1 kcal/mol, the results in Table 2 showed modest variation. Thus, the

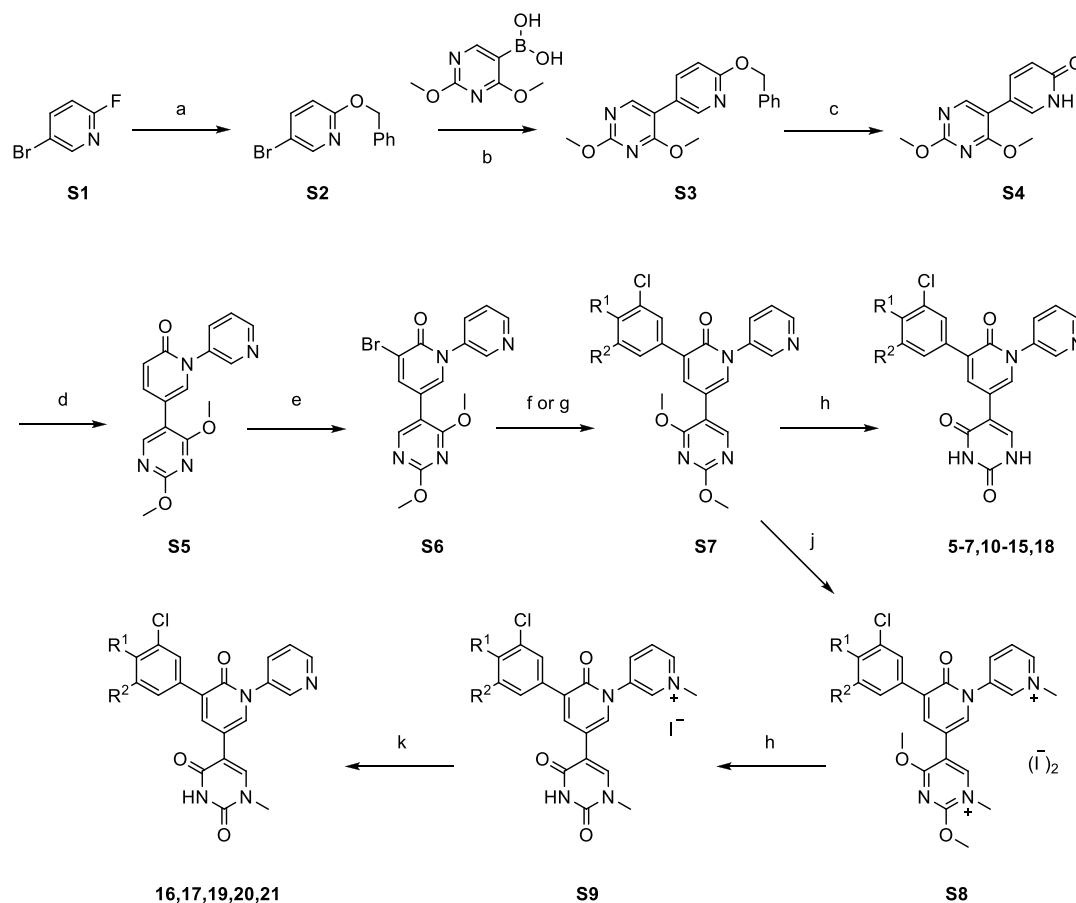
expectation was that multiple heterocycles should be viable, though there is some favoring of having an oxygen or sulfur atom at position 5 (5O and 5S). The most promising compound appeared to be the 4-methyl-5-thiazolyl analogue (3N5S).

Ultimately, it was decided to focus on the uracil subseries since the cyanophenyl analogues are usually weaker M^{Pro} inhibitors.⁸ Furthermore, in initial testing for off-target activity, including inhibition of cytochrome P450 enzymes, the uracil-containing compounds were superior. On the basis of the FEP results and toxicity concerns for furans and thiophenes,^{19,20} synthetic efforts were directed to oxazole and thiazole analogues. An attempt to prepare the 2-imidazole analogue (2N5N) was not successful. An overview of the syntheses of the uracil analogues is provided in Scheme 1, and full details are provided in the Supporting Information. Briefly, 5-bromo-2-fluoropyridine underwent an S_NAr reaction to afford S2, which after Suzuki cross-coupling and deprotection yielded S4. Chan–Evans–Lam coupling²¹ and bromination then yielded S6. This key intermediate was coupled either with commercially available arylboronic acids or with arylboronic acid pinacol esters, which were prepared in a one-pot two-step sequence, to afford S7. The target compounds 5–7, 10–15, and 18 were prepared by demethylation of S7, or S7 was further methylated and demethylated to yield 16, 17, 19, 20, and 21.

The synthesized compounds were all initially tested for their ability to inhibit the proteolytic activity of recombinant SARS-CoV-2 M^{Pro}, as previously described.^{7,8,22,23} The substrate (DabcyL-KTSAVLQJSGFRKM-E(Edans-NH₂); GL Biochem), when cleaved, generates a product containing a free, fluorescent Edans group. Fluorescence measurements used an excitation wavelength of 360 nm and emission wavelength of 460 nm with baseline subtraction for intrinsic fluorescence of each compound and the uncleaved FRET substrate. All of the tested compounds had purities of at least 95% based on HPLC, and all of the measurements were performed in triplicate and averaged.

To begin, compound 8 with a cyclopentylmethoxy substituent was prepared to continue the 2–4 series and to consider a saturated five-membered ring in the S4 site. With an IC₅₀ of 0.328 μ M (Table 1), it turned out to be 2-fold less potent than the cyclopropylmethoxy analogue 3. Then, for the 5-methyl-4-oxazolyl analogues, both the cyanophenyl (9) and uracilyl (10) alternatives were prepared and yielded very similar IC₅₀ values of 0.083 and 0.085 μ M, respectively. 11, the 4-methyl-5-oxazolyl isomer of 10, was also prepared and was a little less active at 0.131 μ M. One thiophene-containing compound, 12, was prepared because of the commercial availability of 2-chloro-3-(chloromethyl)thiophene; this compound was very potent, with an IC₅₀ of 0.027 μ M. It was gratifying that the closely related thiazole 13 was also very potent at 0.042 μ M.

Importantly, it was possible to obtain a high-resolution (1.9 Å) X-ray crystal structure for the complex of thiazole 13 with SARS-CoV-2 M^{Pro}. As shown in Figure 2, the crystal structure confirmed the expectations from the modeling, with clear placement of the methyl group in the S4 site between the side chains of Met165 and Leu167. There are five protein–ligand hydrogen bonds: the pyridinone carbonyl oxygen with Glu166 N (2.81 Å), the pyridine nitrogen with His163 (2.99 Å), and the uracil O–NH–O edge with the NH of Cys145 (3.47 Å) and the backbone O and NH of Thr26 (3.50 and 3.29 Å, respectively). An edge-to-face aryl–aryl interaction between the chlorophenyl ring and His41 and a short (2.93 Å) contact between the uracil O4 and the nitrogen atom of Gly143 are also notable. However, the angular aspects of the latter contact are not consistent with a

Scheme 1. General Synthesis of the Uracil-Containing Inhibitors^a

^aReagents and conditions: (a) benzyl alcohol, NaH, anhydrous THF, 0 to 70 °C; (b) Cs₂CO₃, PdCl₂(PPh₃)₂, DMF, 80 °C, N₂; (c) 10% Pd/C, MeOH/H₂O (10/1 v/v), H₂, 40 °C; (d) 3-pyridylboronic acid, Cu(OAc)₂, TMEDA, anhydrous DMF, air bubbled, rt; (e) NBS, dry DMF, rt; (f) arylboronic acid, K₂CO₃, PdCl₂(PPh₃)₂, DMF, 120 °C, N₂; (g) (i) aryl bromide, KOAc, PdCl₂(PPh₃)₂, B₂Pin₂, anhydrous DMF, 80 °C, N₂; (ii) MeOH, DMF, K₂CO₃, 120 °C, N₂; (h) LiCl, pTsOH, anhydrous DMF, 80 °C; (j) MeI, MeCN, 60 °C; (k) TBAB, diglyme, 130 °C.

hydrogen bond; rather, the NH of Gly143 is hydrogen-bonded with the side-chain carbonyl oxygen atom of Asn142 (2.68 Å). From a force-field optimization of the 13–M^{Pro} complex, the most favorable raw interactions between the inhibitor and protein residues are in the order Glu166 (best), Met165, Gln189, His41, and Cys145, i.e., the S2–S4 region. Net effects on binding would require consideration of desolvation.

In the previous work,⁸ replacement of the terminal methyl group in 2 and 5 with trifluoromethyl (4 and 7) produced significant gains in activity, and some benefits from reduced metabolism might also be expected. Thus, 14, the trifluoromethyl analogue of oxazole 11, was prepared and did yield a small increase in activity, with an IC₅₀ of 0.105 μM. It was also possible to synthesize the desired (Table 2, 3N5S) 5-thiazolyl analogue with a CF₃ group at the 4-position, 15. Indeed, this compound is a very potent inhibitor of M^{Pro}, with an IC₅₀ of 0.038 μM.

By this point and from the previous work,⁸ it had become apparent that although some of the inhibitors had IC₅₀ values below 0.1 μM, including 15, they showed little or no activity in virally infected Vero E6 cellular assays. A likely possibility seemed to be that the uracil group rendered the compounds sufficiently polar that there might be problems with low cell permeability. To test this idea, it was decided to reduce the polarity and hydrogen-bonding needs by methylating N1 of the

uracil group and also to monitor the effects with parallel artificial membrane permeation assay (PAMPA) measurements using hydrophobic poly(vinylidene difluoride) (PVDF) membranes.²⁴

Thus, N-methylated analogues (16, 17, and 19) of some of the previously reported potent inhibitors (6, 7, and 18) were prepared along with 20 and 21, the N-methylated analogues of 14 and 15. The synthetic route to 21, which is outlined in Scheme 2, culminates in a Mitsunobu–Suzuki sequence to yield the protected uracil, which is methylated and demethylated as in Scheme 1. As listed in Table 1, N-methylation increased the IC₅₀ values by 2–3-fold, though 16, 17, 19, and 21 remain very potent at 0.061, 0.059, 0.044, and 0.061 μM, respectively. The details of the PAMPA assay are provided in the Supporting Information; however, theophylline, diclofenac, and chloramphenicol were used as controls and yielded permeability results consistent with literature ranges of (0.3–0.7) × 10^{−6}, (3–5) × 10^{−6}, and (5–5.5) × 10^{−6} cm/s, respectively. Results for 11 M^{Pro} inhibitors are recorded in Table 3 and range from 0.24 × 10^{−6} to 4.27 × 10^{−6} cm/s. The permeabilities of the three cyanophenyl-containing compounds (3, 4, and 9) are good (>3 × 10^{−6} cm/s), while they are low (<0.8 × 10^{−6} cm/s) for the three unmethylated uracil-containing compounds (11, 14, and 18). N-Methylation significantly improved the permeabilities, such that those of 16, 17, 19, 20, and 21 are all above 1 × 10^{−6} cm/s.

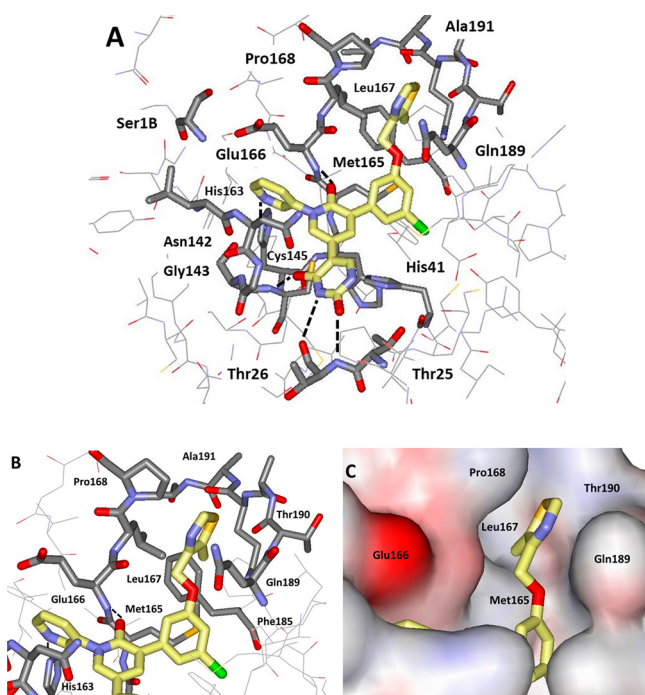


Figure 2. (A) Crystal structure of the complex of **13** with M^{Pro} . Carbon atoms of the ligand are shown in light yellow. Hydrogen bonds between the ligand and protein are noted with dashed lines. The resolution is 1.9 Å. Deposited in the PDB with ID 7N44. (B) Close-up of the S3–S4 channel with placement of the methyl group in the S4 site. (C) Surface view with coloring of the protein by atom type.

The results for **11**, **14**, and **20** are interesting: the permeability of **11** doubles upon replacement of the methyl group by a trifluoromethyl group on the oxazole ring and then doubles again upon N-methylation of the uracil ring to a value of 1.03×10^{-6} cm/s for **20**. Similarly, the permeability of **18** doubles to 1.50×10^{-6} cm/s for N-methylated **19**. As discussed below, a PAMPA result above ca. 0.7×10^{-6} cm/s appears to be necessary for a compound to show activity in the Vero E6 cell assays.

Aqueous solubilities were also measured for 11 compounds, as reported in Table 3, using a standard shake-flask procedure in

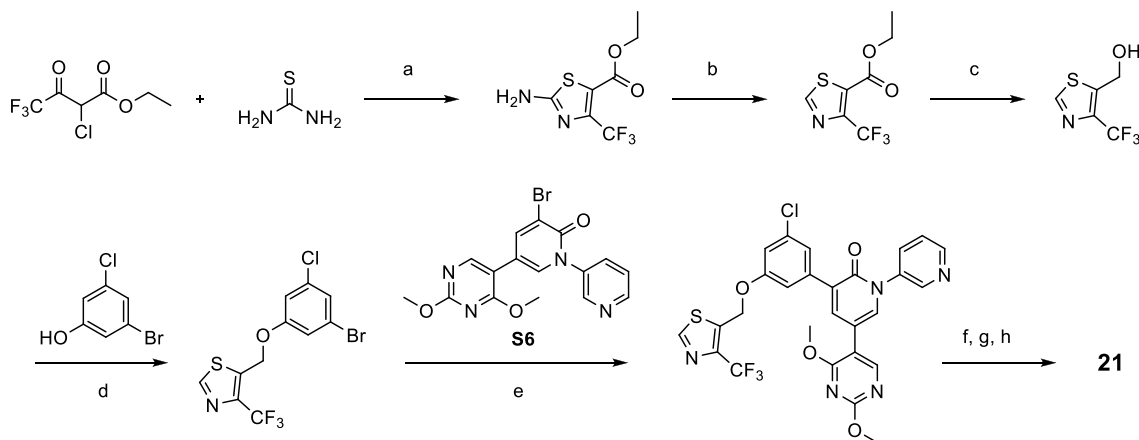
Table 3. Measured PAMPA Permeabilities (in 10^{-6} cm/s) and Aqueous Solubilities (in $\mu\text{g/mL}$)

compd	PAMPA	aq. sol.
3	4.27 ± 0.07	3 ± 2
4	4.0 ± 1.9	25.0 ± 0.1
9	3.04 ± 0.09	13.1 ± 0.3
10	ND	7.6 ± 0.7
11	0.24 ± 0.02	167.7 ± 1.1
14	0.57 ± 0.09	ND
16	3.25 ± 0.46	14.2 ± 0.7
17	2.26 ± 0.14	57.0 ± 0.4
18	0.73 ± 0.05	21.8 ± 0.9
19	1.50 ± 0.59	116.5 ± 8.8
20	1.03 ± 0.18	34.5 ± 0.3
21	1.16 ± 0.32	24.8 ± 1.4

Britton–Robinson buffer at pH 6.5.^{25,26} With the exception of **3**, the results are all in the range observed for oral drugs.²⁷ **11** is the most soluble compound but has low permeability, while the final compounds **16**, **17**, and **19–21** show both acceptable solubility and permeability. The curiously much greater solubility of **11** versus its isomer **10** was fully reproducible and consistent with observations from handling the compounds; it may arise from significantly different arrangements in the crystalline state with intermolecular hydrogen bonding retarded by the methyl group adjacent to the azole nitrogen atom in **11**.

Finally, multiple compounds were tested for inhibition of SARS-CoV-2 replication in Vero E6 cells. Inhibition of viral replication was tested in several cellular assays, as detailed in the Supporting Information. These include a rapid screening replicon assay using baby hamster kidney (BHK) cells with noninfectious SARS-CoV-2, in which the spike protein in the viral genome is replaced with a nanoluciferase reporter, allowing the ability to multiplex in 96-well plates and assess inhibition of viral replication in 24 h. In parallel, the compound general cytotoxicity in either Vero E6 cells or normal human bronchial epithelial (NHBE) cells can be assessed using 3-(4,5-dimethylthiazol-2-yl)-2,5-diphenyltetrazolium bromide (MTT)^{8,28} or alamarBlue dyes as readouts.²⁸ Also, assays using infectious SARS-CoV-2 were performed to examine the

Scheme 2. Synthesis of the Precursor of **21**^a



^aReagents and conditions: (a) DMF, 120 °C; (b) isoamyl nitrite, anhydrous 1,4-dioxane, 85 °C; (c) LiAlH_4 , THF, 0 °C to rt, N_2 ; (d) ADPP, $n\text{-Bu}_3\text{P}$, toluene, 60 °C; (e) (i) KOAc, $\text{PdCl}_2(\text{PPh}_3)_2$, B_2Pin_2 , anhydrous DMF, 80 °C, N_2 ; (ii) MeOH, DMF, K_2CO_3 , 120 °C, N_2 ; (f) MeI, MeCN, 60 °C; (g) LiCl, pTfOH, anhydrous DMF, 80 °C; (h) TBAB, diglyme, 130 °C.

Table 4. Enzyme Inhibition (IC₅₀), Anti-SARS-CoV-2 Activity (EC₅₀), and Cell Cytotoxicity (CC₅₀) (in μM)

compd	IC ₅₀	EC ₅₀		CC ₅₀	
		replicon	infectious virus	Vero E6	NHBE
remdesivir	—	0.59 ± 0.25	0.77, ^a 2.1 ^b	72 ± 28 ^g	41 ± 2 ^g
2	0.140 ± 0.020 ^g	1.51 ± 0.01	1.5 ^{c,g}	22 ± 7.2 ^g	20 ± 2 ^g
3	0.170 ± 0.020 ^g	1.76 ± 0.31	0.98 ^{c,g}	>100 ^g	>100 ^g
4	0.120 ± 0.006 ^g	1.20 ± 0.20	1.1 ± 0.5 ^g	22 ± 8 ^g	25 ± 5 ^g
9	0.083 ± 0.023	0.73 ± 0.26	1.7 ± 0.1 ^h	ND ^e	ND ^e
13	0.042 ± 0.015	>40	ND ^e	>100	22
14	0.105 ± 0.013	NA ^d	ND ^e	>100	>100
15	0.038 ± 0.015	NA ^d	ND ^e	>100	>100
16	0.061 ± 0.007	0.53 ± 0.23	1.2	82	>100
17	0.059 ± 0.014	0.82 ± 0.28	ND ^e	>100	ca. 95
18	0.028 ± 0.007	3.2 ± 1.0	ca. 1	>80	>95
19	0.044 ± 0.009	0.175 ± 0.005	0.08 ^b	>32.5 ^f	>32.5 ^f
21	0.061 ± 0.011	1.08	ND ^e	>100	>100

^aFrom ref 30. ^balamarBlue. ^cPlaque Assay. ^dNA = not active. ^eND = not determined. ^fLimited by the solubility in DMSO. ^gFrom ref 8. ^hMTT.

cytopathic effect in Vero E6 cells in the lower-throughput viral plaque assay²⁹ or using MTT or alamarBlue readout. The results from repeated individual assays are summarized in Table 4; only the plaque assay and CC₅₀ results for remdesivir, 2, 3, and 4 were previously reported.⁸ It should be noted that comparisons with remdesivir are complicated by the fact that it is a prodrug that requires activation by enzymatic hydrolysis and intracellular phosphorylation.

The prior cyanophenyl-containing protease inhibitors 2–4 and the polymerase inhibitor remdesivir have similar activities against SARS-CoV-2, with EC₅₀ values of 0.6–2 μM. The cyanophenyl-containing oxazole 9 showed similar activity in the plaque assay, though greater potency was indicated in the replicon results. Azoles 14 and 15 are not active in the replicon assay in spite of their IC₅₀ values of 0.105 and 0.038 μM (Table 1). This can now be attributed with confidence to poor cell permeability, as reflected in the PAMPA result for 14 (Table 3). The other unmethylated uracil, 18, is a little more permeable and gives an EC₅₀ of 3.2 μM in the replicon assay. Improved results are found for the N-methylated compounds 16, 17, 19, and 21. In particular, 19 is strikingly potent, with EC₅₀ values of 0.175 μM in the replicon assay and 0.08 μM with infectious SARS-CoV-2. These potent compounds also show negligible cytotoxicity in both Vero E6 and NHBE cells.

In conclusion, the prior work on pyridinone inhibitors of the main protease of SARS-CoV-2 has been expanded to include five-membered-ring heterocycles as substituents for filling the S3–S4 channel. Thirteen new compounds were reported, with eight giving IC₅₀ results for enzyme inhibition in the range 0.027–0.085 μM. Projection of a methyl substituent on the azoles into the S4 site was confirmed by the crystal structure for the complex of thiazole 13 with M^{Pro}. Cell permeability was recognized as a problem for antiviral activity in Vero E6 cells for some of the potent enzyme inhibitors. This was well-reflected in PAMPA measurements and remedied by N-methylation of the uracil group. The outcome was notable improvement in antiviral activity for 16, 17, 19, and 21. Compound 19 is particularly compelling; it is an order of magnitude more potent than remdesivir with no apparent cytotoxicity and high aqueous solubility.

■ ASSOCIATED CONTENT

Supporting Information

The Supporting Information is available free of charge at <https://pubs.acs.org/doi/10.1021/acsmchemlett.1c00326>.

Details for the synthetic procedures, compound characterization, computations, assays, and crystallographic results (PDF)

Accession Codes

Coordinates for the crystal structure (Figure 2) have been deposited in the Protein Data Bank with ID 7N44.

■ AUTHOR INFORMATION

Corresponding Authors

Karen S. Anderson — Department of Pharmacology and Department of Molecular Biophysics and Biochemistry, Yale University School of Medicine, New Haven, Connecticut 06520-8066, United States; orcid.org/0000-0003-3433-0780; Email: karen.anderson@yale.edu

William L. Jorgensen — Department of Chemistry, Yale University, New Haven, Connecticut 06520-8107, United States; orcid.org/0000-0002-3993-9520; Email: william.jorgensen@yale.edu

Authors

Chun-Hui Zhang — Department of Chemistry, Yale University, New Haven, Connecticut 06520-8107, United States

Krasimir A. Spasov — Department of Pharmacology, Yale University School of Medicine, New Haven, Connecticut 06520-8066, United States

Raquel A. Reilly — Department of Pharmacology, Yale University School of Medicine, New Haven, Connecticut 06520-8066, United States

Klarissa Hollander — Department of Pharmacology and Department of Molecular Biophysics and Biochemistry, Yale University School of Medicine, New Haven, Connecticut 06520-8066, United States

Elizabeth A. Stone — Department of Chemistry, Yale University, New Haven, Connecticut 06520-8107, United States; orcid.org/0000-0002-2253-3452

Joseph A. Ippolito — Department of Chemistry, Yale University, New Haven, Connecticut 06520-8107, United States

Maria-Elena Liosi — Department of Chemistry, Yale University, New Haven, Connecticut 06520-8107, United States

Maya G. Deshmukh – Department of Pharmacology and M.D.–Ph.D. Program, Yale University School of Medicine, New Haven, Connecticut 06520-8066, United States; orcid.org/0000-0002-3704-3229

Julian Tirado-Rives – Department of Chemistry, Yale University, New Haven, Connecticut 06520-8107, United States; orcid.org/0000-0001-7330-189X

Shuo Zhang – Department of Microbial Pathogenesis, Yale University School of Medicine, New Haven, Connecticut 06536-0812, United States

Zhuobin Liang – Department of Molecular, Cellular, and Developmental Biology, Yale University School of Medicine, New Haven, Connecticut 06520-8066, United States

Scott J. Miller – Department of Chemistry, Yale University, New Haven, Connecticut 06520-8107, United States; orcid.org/0000-0001-7817-1318

Farren Isaacs – Department of Molecular, Cellular, and Developmental Biology, Yale University School of Medicine, New Haven, Connecticut 06520-8066, United States; orcid.org/0000-0001-8615-8236

Brett D. Lindenbach – Department of Microbial Pathogenesis, Yale University School of Medicine, New Haven, Connecticut 06536-0812, United States

Complete contact information is available at:

<https://pubs.acs.org/10.1021/acsmchemlett.1c00326>

Author Contributions

[†]C.-H.Z. and K.A.S. contributed equally to this work.

Notes

The authors declare the following competing financial interest(s): Yale University has submitted a preliminary patent application on the compounds.

ACKNOWLEDGMENTS

The M^{Pro} plasmid was kindly provided by the Hilgenfeld lab.²³ This work was supported by the U.S. National Institutes of Health (GM32136, AI087925) and by CoReCT Pilot Grants from the Yale University School of Medicine. E.A.S. acknowledges support through the NSF Graduate Research Fellowship Program. S.J.M. acknowledges support from the U.S. National Institutes of Health (R35 GM132092). Crystal screening was conducted with support from the Yale Macromolecular X-ray Core Facility (1S10OD018007-01). This research used resources AMX of the National Synchrotron Light Source II, a U.S. Department of Energy (DOE) Office of Science User Facility operated for the DOE Office of Science by Brookhaven National Laboratory under Contract DE-SC0012704. The Life Science Biomedical Technology Research resource is primarily supported by the National Institutes of Health, National Institute of General Medical Sciences (NIGMS) through a Center Core P30 Grant (P30GM133893) and by the DOE Office of Biological and Environmental Research (KP1605010). This work is also based upon research conducted at the Northeastern Collaborative Access Team beamlines, which are funded by the NIGMS (P30 GM124165). The Eiger 16M detector on the 24-ID-E beamline is funded by an NIH-ORIP HEI grant (S10OD021527). This research used resources of the Advanced Photon Source, a DOE Office of Science User Facility operated for the DOE Office of Science by Argonne National Laboratory under Contract DE-AC02-06CH11357.

REFERENCES

- (1) Wu, F.; Zhao, S.; Yu, B.; Chen, Y.-M.; Wang, W.; Song, Z.-G.; Hu, Y.; Tao, Z.-W.; Tian, J.-H.; Pei, Y.-Y.; Yuan, M.-L.; Zhang, Y.-L.; Dai, F.-H.; Liu, Y.; Wang, Q.-M.; Zheng, J.-J.; Xu, L.; Holmes, E. C.; Zhang, Y.-Z. A New Coronavirus Associated with Human Respiratory Disease in China. *Nature* **2020**, *579*, 265–269.
- (2) Morse, J. S.; Lalonde, T.; Xu, S.; Liu, W. R. Learning from the Past: Possible Urgent Prevention and Treatment Options for Severe Acute Respiratory Infections Caused by 2019-nCoV. *ChemBioChem* **2020**, *21*, 730–738.
- (3) Halford, B. To Conquer COVID-19, Create the Perfect Pill. *Chem. Eng. News* **2021**, *99* (19), 28–31.
- (4) Xiong, M.; Su, H.; Zhao, W.; Xie, H.; Shao, Q.; Xu, Y. What Coronavirus 3C-Like Protease Tells Us: From Structure, Substrate Selectivity, to Inhibitor Design. *Med. Res. Rev.* **2021**, *41*, 1965–1998.
- (5) Mengist, H. M.; Mekonnen, D.; Mohammed, A.; Shi, R.; Jin, T. Potency, Safety, and Pharmacokinetic Profiles of Potential Inhibitors Targeting SARS-CoV-2 Main Protease. *Front. Pharmacol.* **2021**, *11*, 630500.
- (6) Dömling, A.; Gao, L. Chemistry and Biology of SARS-CoV-2. *Chem.* **2020**, *6*, 1283–1295.
- (7) Ghahremanpour, M. M.; Tirado-Rives, J.; Deshmukh, M.; Ippolito, J. A.; Zhang, C.-H.; Cabeza de Vaca, I.; Liosi, M.-E.; Anderson, K. S.; Jorgensen, W. L. Identification of 14 Known Drugs as Inhibitors of the Main Protease of SARS-CoV-2. *ACS Med. Chem. Lett.* **2020**, *11*, 2526–2533.
- (8) Zhang, C.-H.; Stone, E. A.; Deshmukh, M.; Ippolito, J. A.; Ghahremanpour, M. M.; Tirado-Rives, J.; Spasov, K. A.; Zhang, S.; Takeo, Y.; Kudalkar, S. N.; Liang, Z.; Isaacs, F.; Lindenbach, B.; Miller, S. J.; Anderson, K. S.; Jorgensen, W. L. Potent Non-Covalent Inhibitors of the Main Protease of SARS-CoV-2 from Molecular Sculpting of the Drug Parampanel Guided by Free-Energy Perturbation Calculations. *ACS Cent. Sci.* **2021**, *7*, 467–475.
- (9) Ghosh, A. K.; Brindisi, M.; Shahabi, D.; Chapman, M. E.; Mesecar, A. D. Drug Development and Medicinal Chemistry Efforts toward SARS-Coronavirus and Covid-19 Therapeutics. *ChemMedChem* **2020**, *15*, 907–932.
- (10) Jorgensen, W. L. Efficient Drug Lead Discovery and Optimization. *Acc. Chem. Res.* **2009**, *42*, 724–733.
- (11) Jorgensen, W. L.; Tirado-Rives, J. Molecular Modeling of Organic and Biomolecular Systems Using BOSS and MCPRO. *J. Comput. Chem.* **2005**, *26*, 1689–1700.
- (12) Robertson, M. J.; Tirado-Rives, J.; Jorgensen, W. L. Improved Peptide and Protein Torsional Energetics with the OPLS-AA Force Field. *J. Chem. Theory Comput.* **2015**, *11*, 3499–3509.
- (13) Jorgensen, W. L.; Tirado-Rives, J. Potential Energy Functions for Atomic-Level Simulations of Water and Organic and Biomolecular Systems. *Proc. Natl. Acad. Sci. U. S. A.* **2005**, *102*, 6665–6670.
- (14) Dodda, L. S.; Cabeza de Vaca, I.; Tirado-Rives, J.; Jorgensen, W. L. LigParGen Web Server: An Automatic OPLS-AA Parameter Generator for Organic Ligands. *Nucleic Acids Res.* **2017**, *45*, W331–W336.
- (15) Wang, L.; Wu, Y.; Deng, Y.; Kim, B.; Pierce, L.; Krilov, G.; Lupyan, D.; Robinson, S.; Dahlgren, M. K.; Greenwood, J.; Romero, D. L.; Masse, C.; Knight, J. L.; Steinbrecher, T.; Beuming, T.; Damm, W.; Harder, E.; Sherman, W.; Brewer, M.; Wester, R.; Murcko, M.; Frye, L.; Farid, R.; Lin, T.; Mobley, D. L.; Jorgensen, W. L.; Berne, B. J.; Friesner, R. A.; Abel, R. Accurate and Reliable Prediction of Relative Protein-Ligand Binding Affinities via Free Energy Calculations: Validation in Prospective Drug Discovery. *J. Am. Chem. Soc.* **2015**, *137*, 2695–2703.
- (16) Jorgensen, W. L. Computer-Aided Discovery of Anti-HIV Agents. *Bioorg. Med. Chem.* **2016**, *24*, 4768–4788.
- (17) Cournia, Z.; Allen, B.; Sherman, W. Relative Binding Free Energy Calculations in Drug Discovery: Recent Advances and Practical Considerations. *J. Chem. Inf. Model.* **2017**, *57*, 2911–2937.
- (18) Jorgensen, W. L.; Chandrasekhar, J.; Madura, J. D.; Impey, R. W.; Klein, M. L. Comparison of Simple Potential Functions for Simulating Liquid Water. *J. Chem. Phys.* **1983**, *79*, 926–935.

- (19) Nelson, S. D. Metabolic Activation and Drug Toxicity. *J. Med. Chem.* **1982**, *25*, 753–765.
- (20) Dang, N. L.; Hughes, T. B.; Miller, G. P.; Swamidass, S. J. Computational Approach to Structural Alerts: Furans, Phenols, Nitroaromatics, and Thiophenes. *Chem. Res. Toxicol.* **2017**, *30*, 1046–1059.
- (21) West, M. J.; Fyfe, J. W. B.; Vantourout, J. C.; Watson, A. J. B. Mechanistic Development and Recent Applications of the Chan-Lam Amination. *Chem. Rev.* **2019**, *119*, 12491–12523.
- (22) Jin, Z.; Zhao, Y.; Sun, Y.; Zhang, B.; Wang, H.; Wu, Y.; Zhu, Y.; Zhu, C.; Hu, T.; Du, X.; Duan, Y.; Yu, J.; Yang, X.; Yang, X.; Yang, K.; Liu, X.; Guddat, L. W.; Xiao, G.; Zhang, L.; Yang, H.; Rao, Z. Structural Basis for the Inhibition of SARS-CoV-2 Main Protease by Antineoplastic Drug Carmofur. *Nat. Struct. Mol. Biol.* **2020**, *27*, 529–532.
- (23) Zhang, L.; Lin, D.; Sun, X.; Curth, U.; Drosten, C.; Sauerhering, L.; Becker, S.; Rox, K.; Hilgenfeld, R. Crystal Structure of SARS-CoV-2 Main Protease Provides a Basis for Design of Improved α -Ketoamide Inhibitors. *Science* **2020**, *368*, 409–412.
- (24) Berben, P.; Bauer-Brandl, A.; Brandl, M.; Faller, B.; Flaten, G. E.; Jacobsen, A. C.; Brouwers, J.; Augustijns, P. Drug Permeability Profiling Using Cell-Free Permeation Tools: Overview and Applications. *Eur. J. Pharm. Sci.* **2018**, *119*, 219–233.
- (25) Baka, E.; Comer, J. E. A.; Takács-Novák, K. Study of Equilibrium Solubility Measurement by Saturation Shake-Flask Method using Hydrochlorothiaide as Model Compound. *J. Pharm. Biomed. Anal.* **2008**, *46*, 335–341.
- (26) Cisneros, J. A.; Robertson, M. J.; Mercado, B. Q.; Jorgensen, W. L. Systematic Study of Effects of Structural Modifications on the Aqueous Solubility of Drug-Like Molecules. *ACS Med. Chem. Lett.* **2017**, *8*, 124–127.
- (27) Jorgensen, W. L.; Duffy, E. M. Prediction of Drug Solubility from Structure. *Adv. Drug Delivery Rev.* **2002**, *54*, 355–366.
- (28) De Meyer, S.; Bojkova, D.; Cinatl, J.; Van Damme, E.; Buyck, C.; Van Loock, M.; Woodfall, B.; Ciesek, S. Lack of Antiviral Activity of Darunavir Against SARS-CoV-2. *Int. J. Infect. Dis.* **2020**, *97*, 7–10.
- (29) Mendoza, E. J.; Manguiat, K.; Wood, H.; Drebot, M. Two Detailed Plaque Assay Protocols for the Quantification of Infectious SARS-CoV-2. *Current Protocols in Microbiology* **2020**, *57*, e105.
- (30) Wang, M.; Cao, R.; Zhang, L.; Yang, X.; Liu, J.; Xu, M.; Shi, Z.; Hu, Z.; Zhong, W.; Xiao, G. Remdesivir and Chloroquine Effectively Inhibit the Recently Emerged Novel Coronavirus (2019-nCoV) In Vitro. *Cell Res.* **2020**, *30*, 269–271.